Transactions of the 15th International Conference on
Structural Mechanics in Reactor Technology (SMiRT-15)
Seoul, Korea, August 15-20, 1999



# Effect of Cladding on Stress Intensity Factors in Reactor Pressure Vessel

Y. J. Kim[1], J. B. Choi[1], J. S. Kim[1], S. N. Choi[2] and K. S. Jang[2]

*1) Sungkyunkwan University, Korea*
*2) Korea Electric Power Research Institute, Korea*

## ABSTRACT

In general, reactor pressure vessels are cladded with stainless steel to prevent corrosion and radiation embrittlement. The ASME Sec. XI specifies that a subclad crack which may be found during the in-service inspection must be considered as a semi-elliptical surface crack when the thickness of cladding is less than 40% of the crack depth. In order to refine the fracture assessment procedures for such subclad cracks, three-dimensional finite element analyses were applied for various subclad cracks embedded in the base metal. A total of 18 crack geometries were analyzed, and the results were compared with those for idealized semi-elliptical surface cracks for two different loading conditions; i.e., internal pressure and pressurized thermal shock. The resulting stress intensity factors for subclad cracks were 50 to 70% less than those for idealized surface cracks. It has been proven that the condition specified on the ASME Sec. XI is overly conservative for subclad cracks which are assumed to be surface cracks.

## 1. INTRODUCTION

In order to maintain the structural integrity of reactor pressure vessel (RPV) under severe operating conditions, it should be designed in accordance with the ASME Boiler and Pressure Vessel Code (ASME) Sec. III[1]. It is, however, possible that micro-cracks may exist as a result of material non-homogeneity and/or welding problems. These micro cracks may grow due to service loading conditions. When a crack is found during the in-service inspection, the structural integrity of RPV should be evaluated according to the fracture mechanics analysis procedure as specified in the ASME Sec. XI[2]. This fracture mechanics analysis procedure is known to be prepared conservatively considering the safety of nuclear power plants. However, overly conservative prediction may lead to unnecessary stop and repair which can cause immense economical loss. Currently, issues regarding this excessive criteria have been raised, and diversified researches are underway to modify the fracture mechanics procedures which are specified in the ASME Sec. XI[3~6].

Most of RPVs are welded along the inside surface with a clad material such as stainless steels, to prevent corrosion and radiation embrittlement. However, subclad cracks may exist at the interface between the base metal and the clad metal due to the material inhomogeneity. If such subclad cracks are detected, they are idealized into either semi-elliptical surface cracks or elliptical subsurface cracks according to the rules given in the ASME Sec. XI, IWB-

3610. These idealized cracks are used for the specified fracture mechanics analysis for RPV integrity evaluation. If this idealization rule is overly conservative, then the fracture mechanics analysis may result in unnecessary repair. Therefore, it is important to investigate the subclad crack behavior based on these idealization rules.

Keeney-Walker et al.[7] performed fracture mechanics analysis on an RPV considering the cladding effect. They showed that the cladding material reduced the stress intensity factors and the *J*-integral by suppressing the crack opening. Recently, subclad cracks considering constraint effects were analyzed by applying two-dimensional finite element analyses[8]. However, to the best knowledge of authors, the quantification of cladding effect on subclad cracks is not available in the open literature.

In this paper, finite element analyses on subclad cracks in RPV were performed to investigate the effects of conservative assumptions introduced in the IWB-3610 on various subclad crack geometries.

## 2. IDEALIZATION OF CRACKS

According to the IWB-3610, cracks which may be found in the clad component are classified into two groups; i.e., the crack and the subsurface cracks. Figs. 1 and 2 show the configuration of surface and subsurface cracks, respectively.

The surface crack is then classified into two groups. One is the crack which lies exclusively in the cladding as shown in Fig. 1 case A. The other is the crack which penetrates the cladding and spreads into the base metal as shown in Fig. 1 case B. According to the IWB-3610, any further analysis is not necessary for case A. For case B, the crack is assumed as a semi-elliptical surface crack with a crack depth of $a$ as illustrated in Fig. 1 case B.

The subsurface cracks are classified into three groups as shown in Fig. 2. Case A shows the subsurface crack which lies in both the clad and the base material. Case B represents the subsurface crack which is contained by the clad material and is classified as subclad crack. Case C is the subsurface crack which lies exclusively in the base material. All three cases should be treated as either a semi-elliptical surface or an elliptical subsurface crack depending on the relation between $S$ and $a$. The condition for idealization is given as,

$$\begin{aligned} &S \geq 0.4a \text{ for subsurface crack} \\ &S < 0.4a \text{ for surface crack} \end{aligned} \tag{1}$$

where $S$ is the minimum distance from the inner surface of cylinder to the crack surface as illustrated in Fig. 2.

When a real subsurface crack is idealized into a semi-elliptical surface crack, the crack depth $a$ is determined as the distance between the inner surface and the deepest point of the crack. This assumption has been adopted in the IWB-3610 for the sake of simple and conservative crack evaluation. In this paper, the subclad crack shown in Fig. 2 case B was considered to investigate the validity of the crack idealization rules given by Eq. (1).

## 3. FINITE ELEMENT MODELLING

In order to investigate the effect of conservative assumptions adopted in the IWB-3610 on the subclad crack idealization, extensive finite element analyses were conducted for the stress intensity factor calculation. The finite element analyses were performed by using ABAQUS Version 5.7[9].

A cladded RPV built in a typical Korean nuclear power plant was chosen for the finite

element modeling. The inner radius was set to 1,994 *mm* with the thickness of 200.2 *mm*. A schematic illustration of the model is given in Fig. 3.

Subclad cracks satisfying the condition of $S < 0.4a$ were modeled for various crack geometries as summarized in Table 1. Corresponding semi-elliptical surface cracks according to the IWB-3610 were designed with the same finite element models by changing the boundary conditions at the clad area. Total of 36 finite element analyses were performed. Due to the symmetric condition, only a quarter of full vessel was modeled. The model was designed with 20 node isoparametric quadratic brick elements with reduced Gaussian integration points. The finite element model consists of 1,984 elements with 9,645 nodes. For the sake of simplicity, residual stresses and contact effects at the interface between base metal and clad metal were ignored. Different material properties were applied to clad material and base metal, respectively, and the rule of mixture governed the deformation behavior. The crack tip was designed with focused elements as shown in the enlarged area of Fig. 4. The elements at the crack tip were designed with quarter-point elements. A typical finite element mesh with a subclad crack embedded is shown in Fig 4.

## 4. FINITE ELEMENT ANALYSES

Finite element analyses were performed in two categories. For the first category, a simple internal pressure was applied considering normal operating condition. For the other one, the pressurized thermal shock was applied to simulate faulted condition. While the internal pressure provides the stress due to mechanical deformation, the pressurized thermal shock gives high stress profile at the wall due to thermal effects, and, for certain cases, it causes plastic behavior in the clad material. In this paper, clad material was assumed to show elastic fully plastic behavior under applied pressurized thermal shock condition.

### 4.1. Category I: Internal pressure

For this category, SA533 Grade B steel and 304 stainless steel were selected for base metal and clad material, respectively. The combination of base metal and clad material is typical for an RPV. Material properties for these two materials are listed in Table 2. For the loading condition, an internal pressure of 15.86 *MPa* was applied on the inner surface of RPV. While the subclad crack was blocked by the clad material, the idealized surface crack was modeled by applying internal pressure on the crack plane. Any change of temperature or thermal stress effect was not included in this category.

### 4.2. Category II: Pressurized thermal shock

For this category, material properties for the base metal and the clad material were adopted from the PTS-ICAS round robin study[10] as specified in Tables 3 and 4, respectively. The applied loading condition was also adopted from the round robin study. The pressurized thermal shock is an accidental condition which varies with increases in time. While thermal conduction was applied on the inner surface of RPV, the outer surface was insulated. The temperature variation was applied on the inner surface of RPV as a function of time and transferred in the wall thickness direction depending on the thermal conductivity coefficients. Any effect of internal pressure was not included.

## 5. FINITE ELEMENT ANALYSIS RESULTS

Stress intensity factors were obtained by converting the resulting *J*-integral directly. Due to the difficulty in obtaining the *J*-integral at the surface point of subclad crack from the

present finite element mesh, the $J$-integral at the deepest point of crack was considered in comparing the analysis results. In general, the stress intensity factor at the deepest crack point, which usually determines the crack instability through the wall thickness direction, is accounted for the deterministic parameter in the fracture mechanics analysis. While accurate stress intensity factors from the surface points were not available from the applied mesh, stress intensity factors decreased for all crack geometries as the point of calculation moves along the crack tip line from the deepest point to the surface point. Therefore, no crack extension was assumed from the surface point prior to the deepest point. Stress intensity factors at the deepest point was obtained by converting the resulting $J$-integral with the following equation representing the plane strain condition.

$$K = \sqrt{\frac{JE}{1-\nu^2}} \tag{2}$$

5.1. Category I: Internal pressure

Stress intensity factors obtained from subclad cracks were compared with those from idealized surface cracks. The differences in stress intensity factors between the subclad cracks and the idealized surface cracks are shown in Figs. 5 and 6 for two different crack lengths, respectively. By increasing the clad thickness from 2.79 *mm* to 5.33 *mm*, the difference in stress intensity factors between the subclad and the idealized surface cracks was slightly increased for both crack lengths. The shallowest cracks with a clad thickness of 5.33 *mm* are idealized into elliptical subsurface cracks according to the IWB-3610. For these idealized cracks, stress intensity factors were calculated by applying equations specified in the ASME Sec. XI, and the results were compared with finite element analysis results for the subclad cracks. Table 5 shows the comparison among three cases. One is an idealized elliptical subsurface crack, another is an assumed semi-elliptical surface crack and the other is a real subclad crack. Geometrical configurations for these cracks are illustrated in Fig. 7. As can be seen in Table 5, semi-elliptical surface cracks resulted in 63% higher stress intensity factors for $c$ = 66.04 *mm* and 75% for $c$ = 114.3 *mm*, than the real subclad cracks, respectively. Idealized subsurface cracks also resulted in 54% higher stress intensity factors for $c$ = 66.04 *mm* and 57% for $c$ = 114.30 *mm*, than the real subclad cracks, respectively. Such a significant difference implies that the idealization rule specified in the IWB 3610 is overly conservative.

Subclad cracks, which are idealized into surface cracks by the IWB-3610, showed considerable differences compared to the corresponding idealized surface cracks. For short cracks, the maximum difference of 57% was observed from the shallowest crack ($p$ = 22.86 *mm*) with a clad thickness of 4.06 *mm*. A minimum difference of 23% was observed for the deepest crack ($p$ = 60.96 *mm*) with a clad thickness of 2.79 *mm*. This tendency is more obvious for long crack ($c$ = 114.3 *mm*) geometries. As shown in Fig. 6, the maximum difference of 68% was observed from the shallowest crack ($p$ = 22.86 *mm*) with a clad thickness of 4.06 *mm*. The minimum difference was 34%.

5.2. Category II: Pressurized thermal shock

In this category, the maximum stress intensity factor was observed from the point passing 3,276 seconds of analysis time for all cases. Therefore, the resulting stress intensity factors at that point were used for the purpose of comparison. The differences between subclad and idealized surface cracks are summarized in Figs. 8 and 9 for two different crack lengths, respectively. By increasing clad thickness from 2.79 *mm* to 5.33 *mm*, the difference in stress intensity factors between subclad and surface cracks slightly increased for both crack lengths.

Stress intensity factors for subclad cracks, which are idealized into surface cracks by the IWB-3610, showed considerable amount of differences compared to those for the corresponding idealized surface cracks. For short cracks, as shown in Fig. 8, the maximum difference of 38% was observed from the shallowest crack ($p$ = 22.86 *mm*) with a clad thickness of 4.06 *mm*. A minimum difference of 6% was observed from the deepest crack ($p$ = 60.96 *mm*) with a clad thickness of 2.79 *mm*. This tendency is more obvious for long crack ($c$ = 114.3 *mm*) geometries. As shown in Fig. 9, the maximum difference of 44% was observed from the shallowest crack ($p$ = 22.86 *mm*) with a clad thickness of 4.06 *mm*, and the minimum difference was 16%.

For all crack geometries, resulting stress intensity factors from subclad cracks were much lower than those from the corresponding surface cracks. This implies that the assumption adopted in the ASME Sec XI, IWB-3610 is overly conservative for these cases.

## 6. CONCLUSIONS

The present paper was prepared to investigate the effect of conservative assumptions introduced in the ASME IWB-3610 on the subclad crack idealization. Total of 36 three-dimensional elastic finite element analyses were performed to calculate stress intensity factors for subclad cracks. Two different loading conditions, the internal pressure and the pressurized thermal shock, were applied to the same finite element meshes. Resulting stress intensity factors at the deepest points were compared with surface crack geometries matching the IWB-3610 idealization rule. For all cases, stress intensity factors for surface cracks were much higher than those for subclad cracks. It has been proved that the IWB-3610 subsurface crack idealization rule produces overly conservative results.

## ACKNOWLEDGEMENT

The authors are grateful for the support provided by a grant from the Korea Electric Power Research Institute and the Safety and Structural Integrity Research Center at the Sungkyunkwan University.

## REFERENCES

1. ASME Boiler and Pressure Vessel Code Section III, *Rules for Construction of Nuclear Power Plant Components.*, 1995.
2. ASME Boiler and Pressure Vessel Code Section XI, *Rules for In-Service Inspection of Nuclear Power Plant Components.*, 1995.
3. Hedden, O.F., "1998 Report on Section XI Activities," *ASME Pressure Vessels and Piping Conference*, PVP-Vol. 360, pp. 165-168, San Diego, 1998.
4. Mohan, R., Wilkowski, G.M., Bass, R. and Bloom, J.M., "A Study of Effects of Pipe Geometry on FAD Curves for Austenitic Stainless Steel and Ferritic Steel Piping Materials," *ASME Journal of Pressure Vessel Technology*, Vol. 120, pp. 86-92, 1998.
5. Roy, S., Grigory, S., Smith, M., Kanninen, M.F. and Anderson, M., "Numerical Simulation of Full-Scale Corroded Pipe Tests With Combined Loading," *ASME Journal of Pressure Vessel Technology*, Vol. 119, pp. 457-466, 1997.
6. Yoon, K.K. and Van Der Sluys, W.A., "Fracture Toughness of Ferritic Steels and Reference Temperature ($T_0$) of ASTM," *ASME Pressure Vessels and Piping Conference*, PVP-Vol. 360, pp. 441-452, San Diego, 1998.
7. Keeney-Walker, J., Bass, B.R. and Pennell, W.E., "Evaluation of the Effects of Irradiated

Cladding on the Behavior of Shallow Flaws Subjected to Pressurized Thermal Shock Loading," *Transactions of the 11th International Conference on Structural Mechanics in Reactor Technology*, Vol. G, pp.195-200, 1991.
8. Miyazaki, N., Ikeda, T. and Ochi, K., "Constraint Effects of Clad on Underclad Crack," *Transactions of the ASME*, Vol. 118, pp. 480-483, 1996.
9. Hibbit, Karlsson & Sorensen, Inc., *ABAQUS/Standard Version 5.7.*, 1997
10. GRS, *Reactor Pressure Vessel Pressurized Thermal Shock International Comparative Assessment Study.*, 1997.

**Table 1 The finite element analysis matrix.**

| No. | $R_i$ [mm] | $t$ [mm] | $S$ [mm] | $p$ [mm] | $c$ [mm] |
|---|---|---|---|---|---|
| 1 | 1994 | 200.2 | 2.79 | 22.86 | 66.04 |
| 2 | | | | | 114.3 |
| 3 | | | | 40.64 | 66.04 |
| 4 | | | | | 114.3 |
| 5 | | | | 60.96 | 66.04 |
| 6 | | | | | 114.3 |
| 7 | | | 4.06 | 22.86 | 66.04 |
| 8 | | | | | 114.3 |
| 9 | | | | 40.64 | 66.04 |
| 10 | | | | | 114.3 |
| 11 | | | | 60.96 | 66.04 |
| 12 | | | | | 114.3 |
| 13 | | | 5.33 | 22.86 | 66.04 |
| 14 | | | | | 114.3 |
| 15 | | | | 40.64 | 66.04 |
| 16 | | | | | 114.3 |
| 17 | | | | 60.96 | 66.04 |
| 18 | | | | | 114.3 |

**Table 2 Material properties for the internal pressure loading.**

| | | |
|---|---|---|
| Base material (SA 533 Grade B) | Young's modulus E [GPa] | 169.6 |
| | Poisson's ratio $\upsilon$ | 0.3 |
| Clad material (Stainless steel) | Young's modulus E [GPa] | 190.3 |
| | Poisson's ratio $\upsilon$ | 0.3 |

**Table 3 Base metal properties for the pressurized thermal shock.**

| Temperature [℃] | 20 | 100 | 200 | 300 | 350 |
|---|---|---|---|---|---|
| Young's modulus E [GPa] | 206 | 199 | 190 | 181 | 172 |
| Poisson's ratio $\upsilon$ | 0.3 | 0.3 | 0.3 | 0.3 | 0.3 |
| Thermal conductivity [W/m K] | 44.4 | 44.4 | 43.2 | 41.8 | 39.4 |
| Specific heat capacity [J/g K] | 0.45 | 0.49 | 0.52 | 0.56 | 0.61 |
| Thermal expansion coeff. [1/K×10^6] | 10.3 | 11.1 | 12.1 | 12.9 | 13.5 |

**Table 4 Clad metal properties for the pressurized thermal shock.**

| Temperature [℃] | 20 | 100 | 200 | 300 | 400 |
|---|---|---|---|---|---|
| Young's modulus E [GPa] | 200 | 194 | 186 | 179 | 172 |
| Poisson's ratio $\upsilon$ | 0.3 | 0.3 | 0.3 | 0.3 | 0.3 |
| Thermal conductivity [W/m K] | 16.0 | 16.0 | 17.0 | 19.0 | 21.0 |
| Specific heat capacity [J/g K] | 0.5 | 0.5 | 0.54 | 0.54 | 0.59 |
| Thermal expansion coeff. [1/K×10^6] | 15.0 | 16.0 | 17.0 | 19.0 | 21.0 |
| Yield strength [MPa] | 320 | 320 | 320 | 320 | 320 |

Table 5 Comparisons of stress intensity factors (case 13 and 14 $S$=5.33 $mm$, $p$=22.86 $mm$). [unit : $MPa\sqrt{m}$]

| C [$mm$] | Surface crack (FEM) | Subclad Crack (FEM) | Difference [%] |
|---|---|---|---|
| 66.04 | 48.20 | 29.55 | 63.11 |
| 114.3 | 54.23 | 31.06 | 74.60 |
| C [$mm$] | Subsurface crack (ASME) | Subclad Crack (FEM) | Difference [%] |
| 66.04 | 45.61 | 29.55 | 54.35 |
| 114.3 | 48.65 | 31.06 | 56.74 |

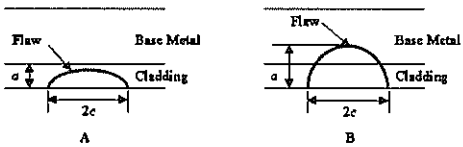


Fig. 1 The surface crack on clad components.

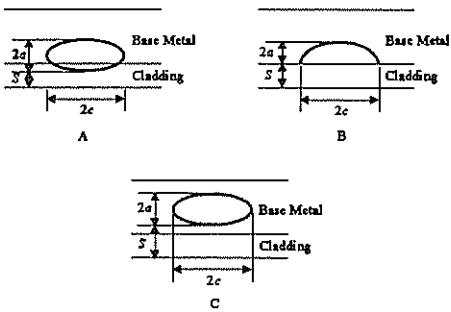


Fig. 2 The subsurface crack on clad components.

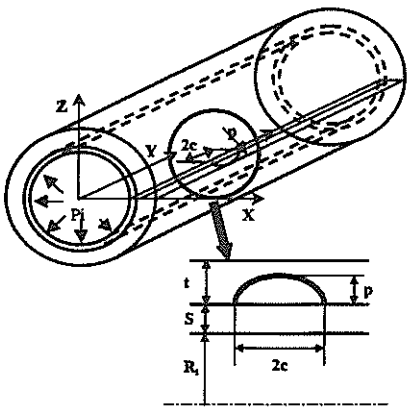


Fig. 3 A schematic illustration of the model.

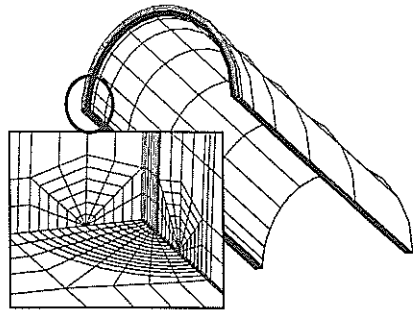

Fig. 4 A typical finite element mesh.

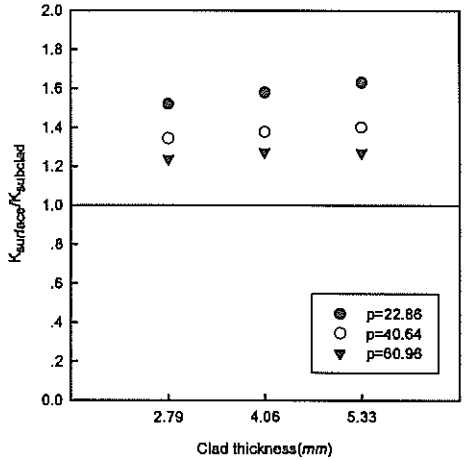


Fig. 5 Comparisons of stress intensity factors ($c$ = 66.04 $mm$).

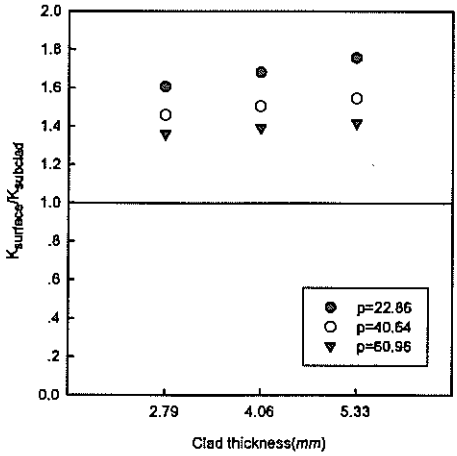


Fig. 6 Comparisons of stress intensity factors ($c$ = 114.3 $mm$).

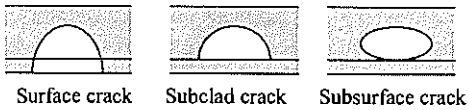


**Fig. 7 Crack geometries specified in Table 5.**

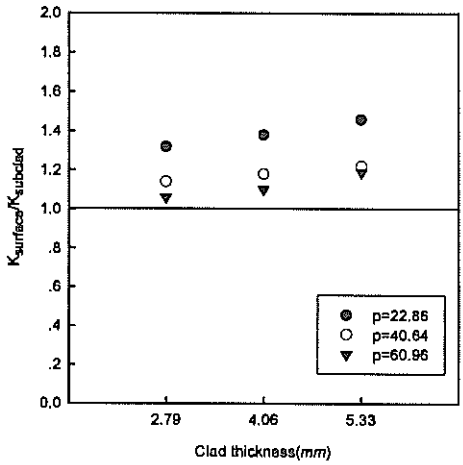


**Fig. 8 Comparisons of stress intensity factors ($c$ = 66.04 *mm*).**

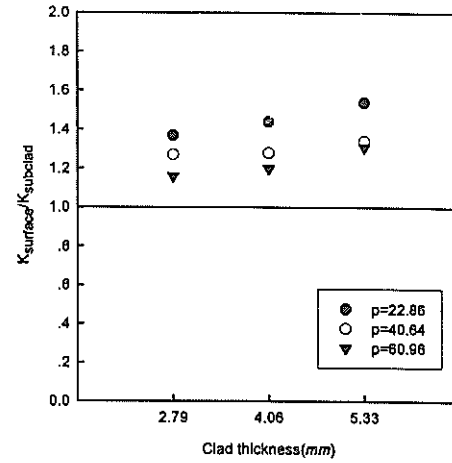


**Fig. 9 Comparisons of stress intensity factors ($c$ = 114.3 *mm*).**